

ORIGINAL ARTICLE

Journal Section

Tracking the Progression & Influence of Beta-Amyloid Plaques Using Percolation Centrality and Collective Influence Algorithm: A Study using PET images

Gautam Kumar Baboo^{1†} | Raghav Prasad^{1†} | Pranav Mahajan^{1†} | Veeky Baths Ph.D.¹

¹Cognitive Neuroscience Lab, Department of Biological Sciences, BITS, Pilani - K. K. Birla Goa Campus, South Goa, Goa, 403726, India

Correspondence

Gautam Kumar Baboo, Department of Biological Science, BITS, Pilani - K.K. Birla Goa Campus, South Goa, Goa, 403726, India
Email: p20130404@goa.bits-pilani.ac.in

Present address

[†]Cognitive Neuroscience Lab, Department of Biological Sciences, BITS, Pilani - K. K. Birla Goa Campus, South Goa, Goa, 403726, India

Funding information

Data usage and analysis for this study is enabled by the Alzheimer's Disease Neuroimaging Initiative - National Institutes of Health Grant U01 AG024904, DOD ADNI, Department of Defense award number W81XWH-12-2-0012

Network analysis allows investigators to explore the many facets of brain networks, particularly the proliferation of disease using graph theory to model the disease movement. The disruption in brain networks in Alzheimer's disease (AD) is due to the abnormal accumulation of beta-amyloid plaques and tau protein tangles. In this study, the potential use of percolation centrality to study the movement of beta-amyloid plaques, as a feature of given PET image-based networks, is studied. The PET image-based network construction is possible using the public access database - Alzheimer's Disease Neuroimaging Initiative, which provided 1522 scans, of which 429 are of AD patients, 583 of patients with mild cognitive impairment, and 510 of cognitively normal. For each image, the Julich atlas provides 121 regions of interest/network nodes. Additionally, the influential nodes for

Abbreviations: AD, Alzheimer's Disease; ANOVA, Analysis of Variance; AV45, Florbetapir (18F-AV-45); CI, Collective Influence; CN, Cognitively Normal; CSF, Cerebrospinal Fluid; EEG, Electroencephalography; FAB, Frontal Assessment Battery; FDG, Fluorodeoxyglucose (18F-FDG); fMRI, functional Magnetic Resonance Imaging; FSL, FMRIB Software Library; GNU, GNU's Not Unix; PCv, Percolation Centrality Value PET, Positron Emission tomography; PIB, Pittsburgh compound B (11C-PIB); MCI, Mild Cognitive Impairment; MEG, Magnetoencephalography; MLR, Multivariate Linear Regression; MMSE, Mini-Mental State Examination; NPIQ, Neuropsychiatric Inventory Questionnaire; OMST, Orthogonal Minimum Spanning Tree.

[†]Equally contributing authors.

each scan are calculated using the collective influence algorithm. Through this study, it is possible to use percolation centrality values to indicate the regions of interest that reflect the disease's spread and show potential use for early AD diagnosis. Analysis of variance (ANOVA) shows the regions of interest for which percolation centrality is a valid measure, irrespective of the tracer type. A multivariate linear regression between the percolation centrality values for each of the nodes and psychometric assessment scores reveals that models Mini-Mental State Examination (MMSE) scores performed better than ones with Neuropsychiatric Inventory Questionnaire (NPIQ) scores as the target variable. Similar to ANOVA, the multivariate linear regression yields regions of interest for which percolation centrality is a good differentiator. Finally, a ranking of the regions of interest is made based on the collective influence algorithm to indicate the anatomical areas strongly influencing the beta-amyloid network.

KEY WORDS

Brain Connectivity, PET, Percolation Centrality, Alzheimer's Disease, Graph theory, Collective Influence

1 | INTRODUCTION

Alzheimer's disease predominantly stands out when it comes to neurodegenerative diseases—affecting the middle-age (early-onset Alzheimer's disease (AD)) and the old-age (Late-onset AD) human population. Current projections are estimated to cost about 2 Trillion US Dollars by 2030[1], affecting 75 million individuals by the same year. The indirect costs are estimated to be about 244 billion US Dollars[2]. With no sight of a cure for AD and with increasing cases, early diagnosis and active management is the key to tackling this disease for now. The ability to predict the disease's progression with high accuracy helps design a suitable treatment regime at an early stage, thereby bringing the disease's management to an affordable cost range.

Current methods of diagnosis of the disease include both non-invasive and invasive techniques of investigations ranging from Positron Emission Tomography (PET) scans or Cerebral Spinal Fluid (CSF) analysis to bedside pen and paper-based questionnaires; each with its pros and cons. The ability to accurately determine that the dementia is due to Alzheimer's is of utmost importance, followed by the ability to indicate the severity of the disease, which is a unique challenge.

A combination of techniques or criteria is currently employed to detect and determine the extent of dementia due to AD. Methods include family history, psychiatric history for cognitive and behavioral changes, which is then followed by psychometric assessments such as Mini-Mental State Examination (MMSE) [3], Frontal Assessment Battery[4], and the Neuropsychiatric Inven-

tory Questionnaire (NPIQ)[5]. Others include Genetic testing[6] for markers of AD, the apolipoprotein-e4 (APOE-e4)[7], or the use of blood testing or brain imaging to rule out dementia due to other factors. The use of PET imaging[8] and lumbar puncture[9] to determine the levels of beta amyloids in either of them beyond the normal levels is the current standard of practice for the determination of dementia due to AD[10, 11].

Positron Emission Tomography or PET imaging involves the use of radiopharmaceuticals such as 2-[¹⁸F] fluoro-2-Deoxy-D-glucose (FDG), florbetapir-fluorine-18 (AV45), or ¹¹C-Pittsburgh compound B (PiB). Among these, FDG has been used for nearly 20 years now. In contrast, AV45 and PiB[12] are comparatively newer and different in terms of the image construction mechanism; both AV45 and PiB bind to the beta-amyloid and vary only in their half-life. AV45 has a half-life of 109.75 minutes and PiB, 20 minutes[13]. In contrast, FDG indicates the neuronal activity based on glucose consumption by the neuronal cells in that region.

The application of network analysis/graph theory to anatomical neural networks has proved useful in understanding the brain connectivity[14, 15] deviations under various psychological and neurological disease states. Network analysis on neuroimaging data such as EEG, MEG, fMRI, and PET scans proves to be useful to show the variation between a cognitively normal population versus other diagnostic states using various graph-theoretic metrics[16, 17].

Network analysis on AD is a practical application wherein it describes the Alzheimer's brain network's behavior. Connectivity analysis using fMRI and EEG data reports provides mixed responses; when comparing AD patients and the control group[18], there is an increase or decrease in the network's connectivity. A reduction in connectivity could explain the cortical atrophy/disruption of the network. An increase could explain the compensatory mechanism[19].

Network Analysis on PET images around AD mainly revolve around learning models or are limited to tracers that focus on the metabolic networks and the associated deviations of these networks[20]. Other meth-

ods include applying algorithms to the raw PET images to recognize patterns to resolve differences between healthy controls and patients with neurodegeneration [21]. Recent methods include genetic and protein markers to improve the predicting the course of the disease[22]. These methods rely on a considerable amount of data points and equally reliable computing hardware; this is currently a challenge. Given that AD diagnosis is a global challenge, a method that works well in a spectrum of nations, from developed countries such as the United States to rural hospitals of southeast Asia or Africa[2].

To address this challenge, we propose applying graph theoretic methods on PET images to understand the advancement of beta-amyloids. The main benefit of adding this method is that

1. This does not introduce any new steps for data collection from the patient and, at the same time
2. adds value to the existing data by computing the percolation centrality of a given node at a given time

Percolation centrality is defined as the proportion of 'percolated paths' that pass through that node; this measure quantifies the relative impact of nodes based on their topological connectivity, as well as their percolated states. In other words, it is one such graph metric that looks at the extent to which a given node within a network has percolated information or can percolate information. The volume of information transmitted via a given node is provided by the values ranging from 0.0 to 1.0[23, 24]. Prior exploration of percolation centrality on disease networks[25, 26, 27, 28] and percolation centrality in disease networks of the brain[29] have shown this as a promising metric for brain network investigation.

The knowledge on the application of percolation centrality on human PET-image based networks is scarce in the present time. This work aims at adding knowledge to the gap. Collective influence, on the other hand, provides a minimum set of nodes or regions of the interest that can transfer information or spread disease with ease with optimal spread[30] based on the optimal

percolation theory. By examining the network for the minimum set of nodes, this set will provide the regions of interests within the brain that optimally move beta-amyloid, which can disrupt the normal functioning of the existing neural networks.

Thus, the ability to detect the disease and predict the rate of progression of the disease at an early stage is imperative. To this end, the study aims to answer two main questions: 1) Can percolation centrality measure be used to determine the percolation of beta-amyloids within the brain? 2) Can the collective influence algorithm provide a minimum set of nodes that are vital to the AD network?

2 | MATERIALS AND METHODS

Based on the tracer agents used for acquiring the PET images, each diagnostic state subset of the dataset is divided into the three available tracers; AV45[31], FDG, and PiB[13].

The patients are categorized into Cognitively normal, with Mild Cognitive Impairment, or having Alzheimer's Disease (AD) based on the psychometric assessments obtained throughout the ADNI study. Next, the PET image is matched with the patient's diagnostic state at the time of the imaging procedure. This provides us with a set of observations for each type of tracer for each patient condition category.

2.0.1 | IRB Waiver Statement

Informed consent from the patients is obtained prior to the assessment carried out by ADNI study team (See ADNI website for details), and this study is a secondary data analysis of the ADNI data collection, which aims at providing a simplified metric to an already diagnosed patient. The data access and usage is within the ADNI data use agreements

2.1 | PET Image preprocessing

Image preprocessing is carried out in two steps:

1. Combining individual frames of the PET image to form a 4D image. This is done using the `fslmerge` utility included in FSL[32].
2. Registering the combined 4D image to MNI[33] space. This is done using FreeSurfer[34]

Given the enormous volume of data, carrying out computation in a sequential manner would be highly time-consuming. Thus, to parallelize this operation, GNU Parallel[?] was used. This could potentially give a maximum speedup of up to 12 times on the system we used for computation (6-core, hyperthreaded Intel i7).

2.2 | PET Image-based Network Construction

The network is constructed using the regions of interest (ROIs) from the Julich Atlas[35, 36, 37]. This atlas provides 121 ROI's, which translates to 121 nodes or vertices in the network. Building networks from the pre-processed images requires the generation of adjacency matrices. This is accomplished by computing the partial correlation values of intensities in the PET images.

The partial correlation is calculated using the correlation between two residuals; the values are computed using $N - 2$ ROIs as co-factors for every pair of ROIs[38]. The partial correlation values serve as the edge weights and constitute the values in the adjacency matrices

The estimation of partial correlations[39] is a computationally intensive task, mainly due to the pre-calculation of residuals before computing cross-correlation; this calculation is done in a time-optimized manner using the R package `ppcor`[40].

Next, the adjacency matrices are thresholded using a Data-Driven Thresholding Scheme Based on Orthogonal Minimal Spanning Trees (OMSTs)[41, 42, 21]. Network thresholding serves to remove inconsequential (or low-impact) edges and reduce the network complexity.

The Networkx[43] Python library is used for network construction from the thresholded adjacency matrices and subsequent percolation centrality computation.

2.3 | Percolation Centrality Computation

Percolation centrality is a nodal metric and is calculated for each node. The percolation centrality for each node v at time t is calculated as shown below:

$$PC^t(v) = \frac{1}{(N-2)} \sum_{s \neq v \neq r} \frac{\sigma_{s,r}(v)}{\sigma_{s,r}} \frac{x_s^t}{[\sum x_v^t] - x_v^t} \quad (1)$$

Where $\sigma_{s,r}$ is the number of shortest paths between nodes s and r ,

$\sigma_{s,r}(v)$ is the number of shortest paths between nodes s and r that pass-through node v ,

x_i^t is the percolation state of node i at time t ,

$x_i^t=0$ indicates a non-percolated node and

$x_i^t=1$ indicates a fully percolated node.

The percolation centrality value is calculated for each network using the inbuilt function of Networkx. This has a worst-case time complexity of $O(n^3)$, where n is the number of nodes in the network. Using a modified form of Brandes' fast algorithm for betweenness centrality[44], the complexity can be reduced to $O(nm)$, where m is the number of edges. However, percolation centrality calculation with target nodes cannot take advantage of this optimization and has a worst-case time complexity of $O(n^3)$ (see supplementary data)

2.4 | Collective Influence Algorithm

The algorithm is on the basis that, given a network: the flow of information within the network is optimal with a minimum number of nodes that weigh heavily on the flow of information through the said network[30]. In the context of this investigation, the small sets of nodes/ROIs would prove to be vital in the movement of beta-amyloid plaques.

The core idea is that the overall functioning of a network in terms of the spread of information (or in our case, movement of beta-amyloid plaques) hinges on a specific set of nodes called influencers. This idea of finding the most influential nodes has been previously used in other contexts, for example, activating influential nodes in social networks to spread information[45]

or de-activating or immunizing influential nodes to prevent large scale pandemics[26, 46]. In recent applications to neuroscience, this method has been used to find nodes essential for global integration of a memory network in rodents[29]. Our work is the first to apply it to study the progression of AD, to the best of our knowledge. In the context of this investigation, these small sets of influential nodes/ROIs would prove to be vital in the movement of beta-amyloid plaques.

We use the Collective Influence (CI) algorithm to pinpoint these most influential nodes, more efficiently than previously known heuristic techniques. CI is an optimization algorithm that aims to find the minimal set of nodes that could fragment the network in optimal percolation, or in a sense, their removal would dismantle the network in many disconnected and non-extensive components. In percolation theory, if we remove nodes randomly, the network would undergo a structural collapse at a critical fraction where the probability that the giant connected component exists is $G = 0$. The optimal percolation is an optimization problem that attempts to find the minimal fraction of influencers q to achieve the result $G(q) = 0$.

3 | RESULTS

Statistical analysis on the percolation centrality values and the patient condition is carried out using the analysis of variance (ANOVA) test.

3.1 | ANOVA

The ANOVA test for each node in the network with the null hypothesis that the mean percolation centrality of that node is the same across the three diagnostic states, CN, MCI, and AD(See Tables 2. & 3).

3.2 | Multivariate Linear regression

A linear regression model between the percolation centrality values for all 121 nodes and psychometric test scores - MMSE and NPIQ - is computed to identify the

regions of interests that can be used as reliable predictors. Instead of performing multiple correlations across all three diagnoses, a multivariate regression analysis using ordinary least squares is carried out, wherein the features are the nodal percolation centrality values and the target variable is the MMSE or NPIQ score(See Table 4.).

4 | DISCUSSION

Graph metrics such as characteristic path length, clustering coefficient, modularity, and hubs have been studied and have provided insights into the brain networks of AD patients and control groups. Some studies have tried to map the progression of MCI to dementia due to AD [47, 18]; thus, network analysis and the various graph metrics have shown potential as a tool to investigate the brain networks.

The reliability of these graph metrics is questionable since they tend to be influenced by other factors such as genetic predisposition, lifestyle, etc. Here, based on the variance analysis and multivariate regression testing, and the percolation centrality graph metric computed using the PET images, it is possible to show the Alzheimer's disease progressing through the beta-amyloid networks.

The intensity of a voxel/node is used to determine if the node is percolated or not; a higher intensity signifies a percolated node, and zero or lower intensity signifies an ability to permeate with ease(See Figure 2.).

It is observed that percolation centrality values of certain areas of the brain, such as inferior and superior parietal lobules, are reliable across the tracers - FDG and PiB, whereas for most other cases, the brain areas differ for each tracer considerably. The variation due to the tracers could be because AV45 and PiB bind to the amyloids, whereas the FDG tracer reflects the neuronal cells' glucose metabolism in a given region of interest. It is also observed that the percolation centrality of Broca's area is a reliable differentiator, which validates previous findings that cognitive impairment affects speech production[48].

Prior research shows that damage to the parietal

lobe is common in AD, which can lead to apraxia[48, 49], which is attested by these results. AD is associated with atrophy of the cornu ammonis, the subfield of the hippocampus, and deficits in episodic memory and spatial orientation[50, 51, 52]. It is observed that the PC values of the hippocampus subiculum are a reliable differentiator across the three stages in the case of FDG tracer.

Comparing the nodes of the network obtained from the ANOVA test with the list of nodes in descending order of influence(see Supporting Information) for each radioisotope across all three diagnoses, Broca's area emerged as a good differentiator in the ANOVA tests. It also emerged as a relatively influential node in the AD condition in the AV45 radioisotope subset. Similarly,

1. The secondary somatosensory cortex/Parietal operculum, inferior parietal lobule, and superior longitudinal fascicle in the AD-FDG subset are responsible for functions such as Fine motor function areas, arithmetic and language functions, and spatial orientation.
2. WM uncinate fascicle, primary somatosensory cortex, visual cortex, amygdala centromedial group, and Insula in the AD-PiB subset, which is involved in the following functions, specific to the retrieval of names of people/things, proprioception, hallucinations, the lack of motivation in patients with AD, autonomic control.
3. In the MCI-AV45 subset. The Premotor cortex; in the MCI-PiB subset, the Inferior parietal lobule, WM uncinate fascicle, and Primary somatosensory cortex. Fine motor skills, mathematical operations, spatial orientation and language functions, retrieval of names, proprioception(See Figure 3.).

The collective influence algorithm yields nine rank lists. These tables contain the ranking of the nodes, from most influential to least, for each patient condition and type of tracer used(see Figure 5.). Moreover, since the influential nodes are identified using optimal percolation theory, it validates percolation centrality as a potential metric for diagnosis.

The PET tracers used for acquiring the images, Pitts-

burgh Compound B (11C- PiB) and Florbetapir (18F-AV-45), are compared to check for which among the two tracers provide a more consistent or reliable PCv. Here, the AV-45 tracer binds with a high affinity to the beta-amyloid plaque, whereas PiB binds to oligomers or protofibrils. A possible explanation for the difference in PCv generated using these tracers would be their binding targets. The use of second-generation tracers can help improve the accuracy and test the applicability of percolation centrality on other neurodegenerative diseases and the possibility of using it in metastatic cancer scenarios.

Unlike AV45 and PiB, which binds to beta-amyloid plaques and tau proteins directly, and thus indicate beta-amyloid plaque concentrations, FDG reflects the regional cerebral metabolic rate for glucose (rCGMr), providing information about the neuronal inactivity [53]. Hence, in a PET image that uses FDG, regions of higher intensity indicate higher neuronal activity. The current pipeline is built for tracers such as AV45 and PiB, which indicate beta-amyloid plaque concentrations directly. However, the pipeline can work with a tracer like FDG with some appropriate modifications, namely: taking the multiplicative inverse of the percolation states of each of the ROIs to reflect the behavior of the FDG tracer(See Figure 4.). The rest of the pipeline requires no change because the edge weights for the beta-amyloid plaque networks are calculated as pairwise partial correlations between the nodal percolation states.

4.1 | Limitations

This study does not give any evidence regarding the disease progression in terms of the ROIs or patient category. However, this can be addressed by increasing the number of observations within each patient category.

By expanding the dataset to include more patients and with comprehensive data that factors in healthy aging shrinkage of the brain, which results in a decrease of the distances of the brain networks, can help improve the reliability of the Percolation Centrality value. This can then provide a setting for testing out other psychological assessments that can be used as early indicators

for dementia due to Alzheimer's disease, thereby tailoring it to specific demographics or population subsets.

5 | CONCLUSION

This study aims to show that percolation centrality is a reliable predictor and identifies the nodes that regulate the movement of beta-amyloid plaque and use them to track the disease.

This work demonstrates that using the existing neuroimaging method, PET-CT, this work can add value with relatively short computation time provided sufficient hardware capability is present. The ability to provide a metric to the extent of the disease state is advantageous to the current world of Alzheimer's. Prolonging life with modern-day medicine pushes patients to a world of medical experiences that deviate from the normal. Being able to show the deviation with a value such as percolation centrality has potential applications.

The reliability of percolation centrality can be improved by addressing the concerns that arise by the factors such as the number of patients and the number of patients within each category, time points of data collection, demographic, and the PET tracers used were the limiting factors. Thus, this study provides the usability of percolation centrality value to determine the state of the patient and also sets the stage for studying other neurodegenerative diseases.

Unlike measures such as hub centrality or betweenness centrality, which provide information regarding a vital vertex/node within a network, the collective influence algorithm provides a minimum set of nodes of the network that are key to the beta-amyloid plaque movement, which can provide information regarding a particular pathway that is susceptible to the disease.

Author Contribution

Gautam Kumar conceived the hypothesis and the design of the study. Pranav explored the potential of collective influence on the network. Both Raghav and Pranav carried out the analysis, and the necessary scripting for the computing of PC values listing of

the influential nodes and statistical analysis and Veekey Baths helped in the manuscript preparation.

Acknowledgements

ADNI for providing the access to the PET images.

Conflict of interest

No competing financial interests exist.

references

- [1] El-Hayek YH, Wiley RE, Khoury CP, Daya RP, Ballard C, Evans AR, et al. Tip of the Iceberg: Assessing the Global Socioeconomic Costs of Alzheimer's Disease and Related Dementias and Strategic Implications for Stakeholders. *Journal of Alzheimer's Disease* 2019;70:1-19.
- [2] 2020 Alzheimer's disease facts and figures. *Alzheimer's and Dementia* 2020;16(3):391-460.
- [3] Tombaugh TN, McDowell I, Kristjansson B, Hubley AM. Mini-Mental State Examination (MMSE) and the Modified MMSE (3MS): A psychometric comparison and normative data. *Psychological Assessment* 1996;8(1):48-59.
- [4] Dubois B, Slachevsky A, Litvan I, Pillon B. The FAB: a Frontal Assessment Battery at bedside. *Neurology* 2000 dec;55(11):1621-1626.
- [5] Cummings JL, Mega M, Gray K, Rosenberg-Thompson S, Carusi DA, Gornbein J. The Neuropsychiatric Inventory: comprehensive assessment of psychopathology in dementia. *Neurology* 1994 dec;44(12):2308-2314.
- [6] Loy CT, Schofield PR, Turner AM, Kwok JBJ. Genetics of dementia. *Lancet (London, England)* 2014 mar;383(9919):828-840.
- [7] Holtzman DM, Herz J, Bu G. Apolipoprotein E and apolipoprotein E receptors: normal biology and roles in Alzheimer disease. *Cold Spring Harbor perspectives in medicine* 2012 mar;2(3):a006312.
- [8] Johnson KA, Minoshima S, Bohnen NI, Donohoe KJ, Foster NL, Herscovitch P, et al. Appropriate use criteria for amyloid PET: a report of the Amyloid Imaging Task Force, the Society of Nuclear Medicine and Molecular Imaging, and the Alzheimer's Association. *Alzheimer's & dementia : the journal of the Alzheimer's Association* 2013 jan;9(1):e-1-16.
- [9] Shaw LM, Arias J, Blennow K, Galasko D, Molinuevo JL, Salloway S, et al. Appropriate use criteria for lumbar puncture and cerebrospinal fluid testing in the diagnosis of Alzheimer's disease. *Alzheimer's & dementia : the journal of the Alzheimer's Association* 2018 nov;14(11):1505-1521.
- [10] McKhann GM, Knopman DS, Chertkow H, Hyman BT, Jack CRJ, Kawas CH, et al. The diagnosis of dementia due to Alzheimer's disease: recommendations from the National Institute on Aging-Alzheimer's Association workgroups on diagnostic guidelines for Alzheimer's disease. *Alzheimer's & dementia : the journal of the Alzheimer's Association* 2011 may;7(3):263-269.
- [11] Sperling RA, Aisen PS, Beckett LA, Bennett DA, Craft S, Fagan AM, et al. Toward defining the preclinical stages of Alzheimer's disease: recommendations from the National Institute on Aging-Alzheimer's Association workgroups on diagnostic guidelines for Alzheimer's disease. *Alzheimer's & dementia : the journal of the Alzheimer's Association* 2011 may;7(3):280-292.
- [12] Landau SM, Thomas BA, Thurfjell L, Schmidt M, Margolin R, Mintun M, et al. Amyloid PET imaging in Alzheimer's disease: a comparison of three radio-tracers. *European journal of nuclear medicine and molecular imaging* 2014 jul;41(7):1398-1407. <https://pubmed.ncbi.nlm.nih.gov/24647577/> <https://www.ncbi.nlm.nih.gov/pmc/articles/PMC4055504/>.
- [13] Yamin G, Teplow DB. Pittsburgh Compound-B (PiB) binds amyloid β -protein protofibrils. *Journal of neurochemistry* 2017 jan;140(2):210-215. <https://pubmed.ncbi.nlm.nih.gov/27943341/> <https://www.ncbi.nlm.nih.gov/pmc/articles/PMC5225051/>.
- [14] Reijneveld JC, Ponten SC, Berendse HW, Stam CJ. The application of graph theoretical analysis to complex networks in the brain. *Clinical Neurophysiology* 2007;118(11):2317-2331.
- [15] Stam CJ, Reijneveld JC, Graph theoretical analysis of complex networks in the brain; 2007.
- [16] Sakkalis V. Modern electroencephalographic assessment techniques: Theory and applications; 2014.
- [17] Vecchio F, Miraglia F, Maria Rossini P. Connectome: Graph theory application in functional brain network architecture. *Clinical Neurophysiology Practice*

- 2017;2:206–213. <https://doi.org/10.1016/j.cnp.2017.09.003>.
- [18] Tijms BM, Wink AM, de Haan W, van der Flier WM, Stam CJ, Scheltens P, et al. Alzheimer's disease: connecting findings from graph theoretical studies of brain networks. *Neurobiology of Aging* 2013;34(8):2023–2036. <http://dx.doi.org/10.1016/j.neurobiolaging.2013.02.020>.
- [19] Wook Yoo S, Han CE, Shin JS, Won Seo S, Na DL, Kaiser M, et al. A network flow-based analysis of cognitive reserve in normal ageing and Alzheimer's disease. *Scientific Reports* 2015;5:1–14. <http://dx.doi.org/10.1038/srep10057>.
- [20] Chung J, Yoo K, Kim E, Na DL, Jeong Y, Glucose Metabolic Brain Networks in Early-Onset vs. Late-Onset Alzheimer's Disease ; 2016. <https://www.frontiersin.org/article/10.3389/fnagi.2016.00159>.
- [21] Klyuzhin IS, Fu JF, Hong A, Sacheli M, Shenkov N, Matarazzo M, et al. Data-driven, voxel-based analysis of brain PET images: Application of PCA and LASSO methods to visualize and quantify patterns of neurodegeneration. *PLoS ONE* 2018;13(11):1–20.
- [22] Gupta Y, Lama RK, Kwon GR, Weiner MW, Aisen P, Weiner M, et al., Prediction and Classification of Alzheimer's Disease Based on Combined Features From Apolipoprotein-E Genotype, Cerebrospinal Fluid, MR, and FDG-PET Imaging Biomarkers ; 2019. <https://www.frontiersin.org/article/10.3389/fncom.2019.00072>.
- [23] Newman MEJ, Watts DJ. Scaling and percolation in the small-world network model. *Physical Review E - Statistical Physics, Plasmas, Fluids, and Related Interdisciplinary Topics* 1999;60(6):7332–7342.
- [24] Piraveenan M, Prokopenko M, Hossain L. Percolation Centrality: Quantifying Graph-Theoretic Impact of Nodes during Percolation in Networks. *PLOS ONE* 2013 jan;8(1):e53095. <https://doi.org/10.1371/journal.pone.0053095>.
- [25] Moore C, Newman MEJ. Epidemics and percolation in small-world networks. *Physical Review E* 2000 may;61(5):5678–5682. <https://link.aps.org/doi/10.1103/PhysRevE.61.5678>.
- [26] Newman MEJ. Spread of epidemic disease on networks. *Physical Review E* 2002 jul;66(1):16128. <https://link.aps.org/doi/10.1103/PhysRevE.66.016128>.
- [27] Piraveenan M, Prokopenko M, Hossain L. Percolation Centrality: Quantifying Graph-Theoretic Impact of Nodes during Percolation in Networks. *PLOS ONE* 2013;8(1).
- [28] Sander LM, Warren CP, Sokolov IM, Simon C, Koopman J. Percolation on heterogeneous networks as a model for epidemics. *Mathematical biosciences* 2002;180:293–305.
- [29] Del Ferraro G, Moreno A, Min B, Morone F, Pérez-Ramírez Ú, Pérez-Cervera L, et al. Finding influential nodes for integration in brain networks using optimal percolation theory. *Nature Communications* 2018;9(1). <http://dx.doi.org/10.1038/s41467-018-04718-3>.
- [30] Morone F, Min B, Bo L, Mari R, Makse HA. Collective Influence Algorithm to find influencers via optimal percolation in massively large social media. *Scientific reports* 2016 jul;6:30062.
- [31] Chopra A, Shan L, Eckelman WC, Leung K, Latterner M, Bryant SH, et al. Molecular Imaging and Contrast Agent Database (MICAD): evolution and progress. *Molecular imaging and biology* 2012 feb;14(1):4–13. <https://europemmc.org/articles/PMC3259264>.
- [32] Jenkinson M, Beckmann CF, Behrens TEJ, Woolrich MW, Smith SM. FSL. *NeuroImage* 2012 aug;62(2):782–790.
- [33] Vizza P, Tradigo G, Messina D, Cascini GL, Veltri P. Methodologies for the analysis and classification of PET neuroimages. *Network Modeling Analysis in Health Informatics and Bioinformatics* 2013;2(4):191–208. <https://doi.org/10.1007/s13721-013-0035-9>.
- [34] Reuter M, Schmansky NJ, Rosas HD, Fischl B. Within-subject template estimation for unbiased longitudinal image analysis. *NeuroImage* 2012 jul;61(4):1402–1418. <https://pubmed.ncbi.nlm.nih.gov/22430496/> <https://www.ncbi.nlm.nih.gov/pmc/articles/PMC3389460/>.
- [35] Kötter R, Mazziotta J, Toga A, Evans A, Fox P, Lancaster J, et al. A probabilistic atlas and reference system for the human brain: International Consortium for Brain Mapping (ICBM). *Philosophical Transactions of the Royal Society of London Series B: Biological Sciences* 2001 aug;356(1412):1293–1322. <https://doi.org/10.1098/rstb.2001.0915>.
- [36] Eickhoff SB, Stephan KE, Mohlberg H, Grefkes C, Fink GR, Amunts K, et al. A new SPM toolbox for combining

- probabilistic cytoarchitectonic maps and functional imaging data. *NeuroImage* 2005 may;25(4):1325–1335.
- [37] Desikan RS, Ségonne F, Fischl B, Quinn BT, Dickerson BC, Blacker D, et al. An automated labeling system for subdividing the human cerebral cortex on MRI scans into gyral based regions of interest. *NeuroImage* 2006 jul;31(3):968–980.
- [38] Madigan D. Graphical models in applied multivariate statistics, by J. Whittaker, John Wiley & Sons, New York, 1990, 448 pp. Price: \$59.95. *Networks* 1994 mar;24(2):125. <https://doi.org/10.1002/net.3230240213>.
- [39] Son SJ, Kim J, Seo J, min Lee J, Park H. Connectivity analysis of normal and mild cognitive impairment patients based on FDG and PiB-PET images. *Neuroscience Research* 2015;98:50–58.
- [40] Kim S. ppcor: An R Package for a Fast Calculation to Semi-partial Correlation Coefficients. *Communications for Statistical Applications and Methods* 2015 nov;22(6):665–674. <http://http://www.csam.or.kr/journal/view.html?doi=10.5351/CSAM.2015.22.6.665>.
- [41] Dimitriadis SI, Salis C, Tarnanas I, Linden DE. Topological Filtering of Dynamic Functional Brain Networks Unfolds Informative Chronnectomics: A Novel Data-Driven Thresholding Scheme Based on Orthogonal Minimal Spanning Trees (OMSTs); 2017. <https://www.frontiersin.org/article/10.3389/fninf.2017.00028>.
- [42] Dimitriadis SI, Antonakakis M, Simos P, Fletcher JM, Papanicolaou AC. Data-Driven Topological Filtering Based on Orthogonal Minimal Spanning Trees: Application to Multigroup Magnetoencephalography Resting-State Connectivity. *Brain connectivity* 2017 dec;7(10):661–670. <https://pubmed.ncbi.nlm.nih.gov/28891322https://www.ncbi.nlm.nih.gov/pmc/articles/PMC6435350/>.
- [43] Hagberg AA, Schult DA, Swart PJ. Exploring Network Structure, Dynamics, and Function using NetworkX. In: Varoquaux G, Vaught T, Millman J, editors. *Proceedings of the 7th Python in Science Conference* Pasadena, CA USA; 2008. p. 11–15.
- [44] Brandes U. A faster algorithm for betweenness centrality. *The Journal of Mathematical Sociology* 2001 jun;25(2):163–177. <https://doi.org/10.1080/0022250x.2001.9990249>.
- [45] Richardson M, Domingos P. Mining Knowledge-Sharing Sites for Viral Marketing. In: *Proceedings of the Eighth ACM SIGKDD International Conference on Knowledge Discovery and Data Mining KDD '02*, New York, NY, USA: Association for Computing Machinery; 2002. p. 61–70. <https://doi.org/10.1145/775047.775057>.
- [46] Pastor-Satorras R, Vespignani A. Epidemic Spreading in Scale-Free Networks. *Phys Rev Lett* 2001 Apr;86:3200–3203. <https://link.aps.org/doi/10.1103/PhysRevLett.86.3200>.
- [47] de Haan W, Mott K, van Straaten ECW, Scheltens P, Stam CJ. Activity Dependent Degeneration Explains Hub Vulnerability in Alzheimer's Disease. *PLoS Computational Biology* 2012;8(8).
- [48] Fernández M, Gobart AL, Balañá M, Group CS. Behavioural symptoms in patients with Alzheimer's disease and their association with cognitive impairment. *BMC neurology* 2010 sep;10:87. <https://pubmed.ncbi.nlm.nih.gov/20920205https://www.ncbi.nlm.nih.gov/pmc/articles/PMC2955564/>.
- [49] Kueper JK, Speechley M, Lingum NR, Montero-Odasso M. Motor function and incident dementia: a systematic review and meta-analysis. *Age and Ageing* 2017 sep;46(5):729–738. <https://doi.org/10.1093/ageing/afw084>.
- [50] Adler DH, Wisse LEM, Ittyerah R, Pluta JB, Ding SL, Xie L, et al. Characterizing the human hippocampus in aging and Alzheimer's disease using a computational atlas derived from ex vivo MRI and histology. *Proceedings of the National Academy of Sciences of the United States of America* 2018;115(16):4252–4257.
- [51] Masurkar AV. Towards a circuit-level understanding of hippocampal CA1 dysfunction in Alzheimer's disease across anatomical axes. *Journal of Alzheimer's disease & Parkinsonism* 2018;8(1):412. <https://pubmed.ncbi.nlm.nih.gov/29928558https://www.ncbi.nlm.nih.gov/pmc/articles/PMC6005196/>.
- [52] Ogawa M, Sone D, Beheshti I, Maikusa N, Okita K, Takano H, et al. Association between subfield volumes of the medial temporal lobe and cognitive assessments. *Heliyon* 2019;5(6):e01828. <http://www.sciencedirect.com/science/article/pii/S2405844018361486>.

- [53] Smailagic N, Vacante M, Hyde C, Martin S, Ukomunne O, Sachpekidis C. ¹F-FDG PET for the early diagnosis of Alzheimer's disease dementia and other dementias in people with mild cognitive impairment (MCI). The Cochrane database of systematic reviews 2015 jan;1(1):CD010632–CD010632. <https://pubmed.ncbi.nlm.nih.gov/25629415/> <https://www.ncbi.nlm.nih.gov/pmc/articles/PMC7081123/>.

6 | FIGURES AND TABLES

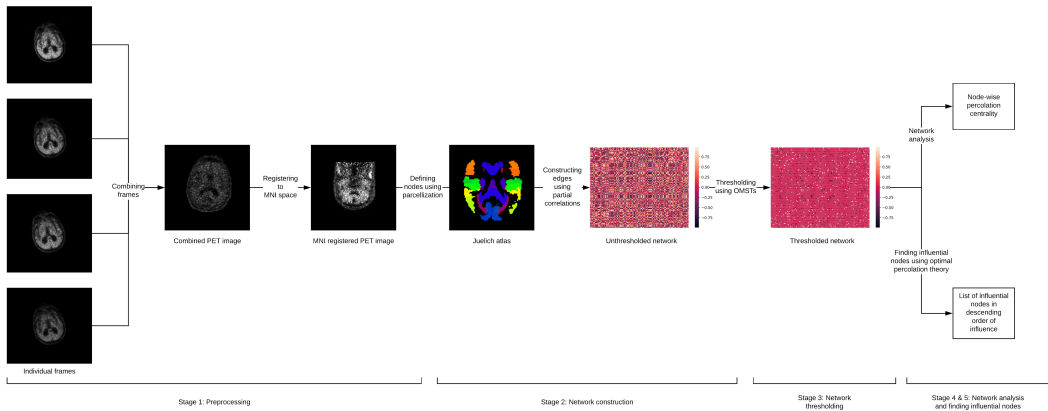


FIGURE 1 The pipeline of the PET-image processing and network construction.

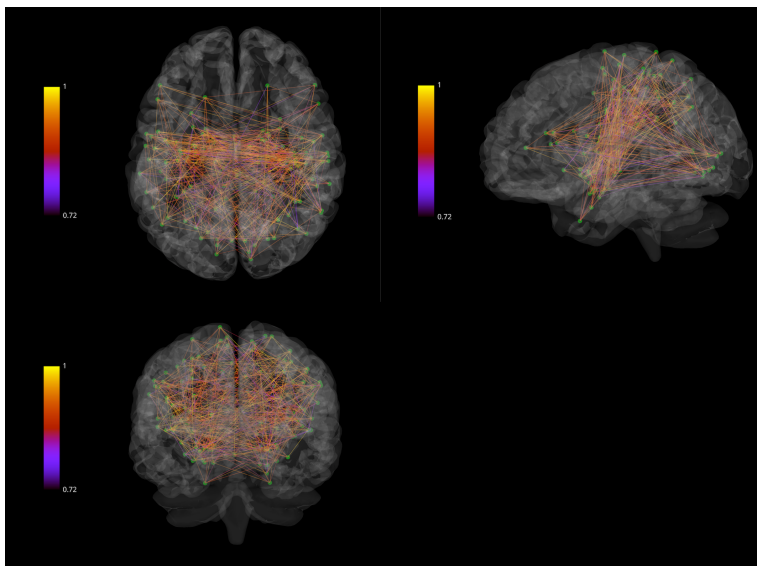


FIGURE 2 A connected network of all the nodes using the Julich Atlas. Green circles indicate the ROIs, the connecting lines indicate the edges with their weights as denoted by the accompanying color bar

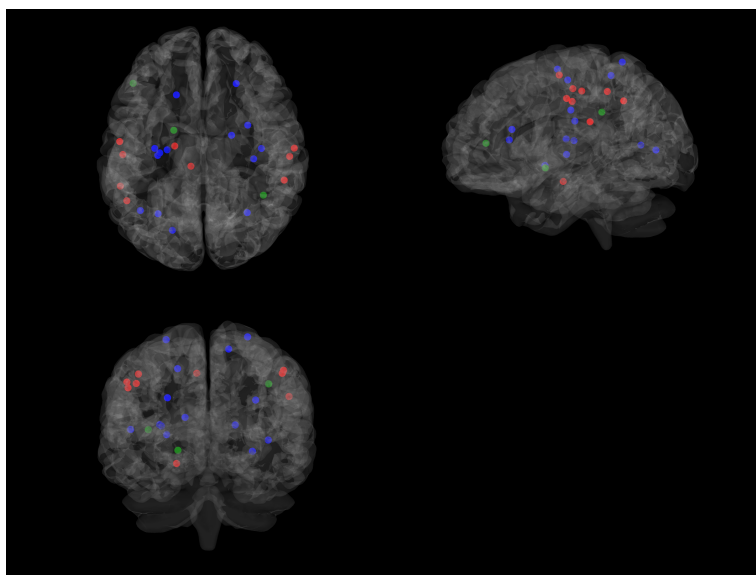


FIGURE 3 Illustrates the findings of the ANOVA analysis. The green circles represent ROIs from AV45 scans with an f-value greater than the AV45 critical f-value, the red circles represent ROIs from FDG scans with an f-value greater than the FDG critical f-value, and the blue circles represent ROIs from PiB scans with an f-value greater than the PiB critical f-value. The critical f-values are tabulated in Table 2.

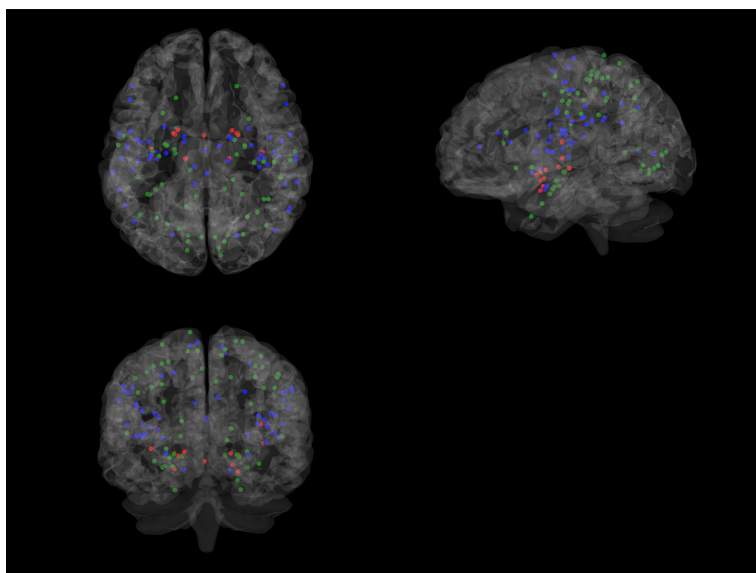


FIGURE 4 Illustrates the ROI's that corresponds to MMSE and NPIQ. The green circles represent ROIs associated with the MMSE psychometric assessment, the red circles represent ROIs associated with the NPIQ psychometric assessment, and the blue circles represent ROIs associated with both MMSE and NPIQ

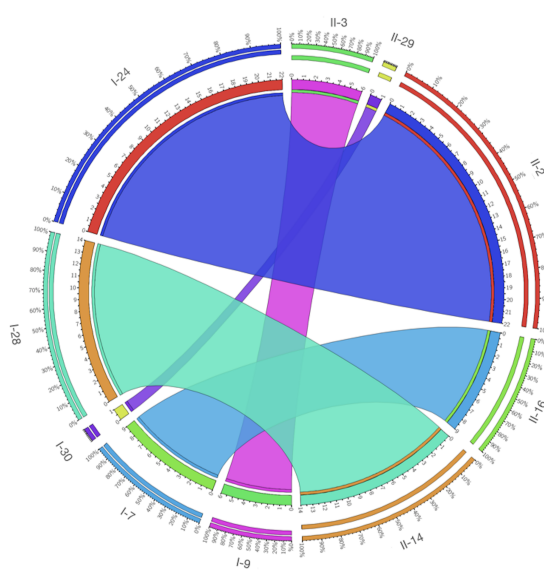


FIGURE 5 CIRCOS plot comparing ROI ranklists of MCI-FDG and MCI-PiB scans

TABLE 1 Distribution of patients

CN			MCI			AD		
AV45	FDG	PiB	AV45	FDG	PiB	AV45	FDG	PiB
272	225	13	98	418	67	117	293	19
M - 127	M - 122	M - 8	M - 62	M - 274	M - 45	M - 68	M - 177	M - 11
F - 145	F - 103	F - 5	F - 36	F - 144	F - 22	F - 49	F - 116	F - 8
Total - 510; M - 257, F - 253			Total - 582; M - 381, F - 202			Total - 429; M - 256, F - 173		

TABLE 2 Number of Scans per tracer type and corresponding critical F-value

Tracer	AV45	FDG	PiB
No. Of scans	487	936	99
Critical f-value	3.005	3.0005	3.042

Supporting Information

TABLE 3 Represents the following nodes that reject the ANOVA null hypothesis.

AV45		
ROI	F-value	p-value
GM Primary somatosensory cortex BA2 L	8.5243	0.0002
GM Broca's area BA45 R	3.2760	0.0386
GM Premotor cortex BA6 L	3.2357	0.0402
FDG		
ROI	F-value	p-value
GM Inferior parietal lobule Pga R	4.0590	0.0176
GM Superior parietal lobule 7A L	3.4849	0.0311
GM Hippocampus subiculum R	3.4807	0.0312
GM Superior parietal lobule 7A R	3.4493	0.0322
GM Inferior parietal lobule PFcm L	3.3303	0.0362
WM Corticospinal tract R	3.0890	0.0460
WM Superior longitudinal fascicle L	3.0716	0.0468
GM Inferior parietal lobule PFt R	3.0531	0.0477
GM Anterior intra-parietal sulcus hIP1 L	3.0235	0.0491
PiB		
ROI	f_value	p_value
GM Inferior parietal lobule PFm R	5.0120	0.0085
WM Uncinate fascicle L	4.8119	0.0102
GM Insula Id1 L	4.3022	0.0162
GM Primary somatosensory cortex BA1 L	4.1049	0.0195
WM Superior occipito-frontal fascicle R	3.9852	0.0217
GM Superior parietal lobule 5Ci R	3.9103	0.0233
GM Visual cortex V5 R	3.7558	0.0269
WM Optic radiation R	3.6645	0.0293
GM Amygdala_centromedial group R	3.5831	0.0316
WM Superior occipito-frontal fascicle L	3.5776	0.0317
WM Superior longitudinal fascicle R	3.4011	0.0374
GM Primary somatosensory cortex BA1 R	3.2338	0.0437
GM Insula Ig2 R	3.2205	0.0443
GM Insula Ig1 R	3.1774	0.0461

TABLE 4 A summary of the MLR models between nodal percolation centrality values and MMSE score, and a list of nodes that have p-value < 0.05

AV45		
Model summary		
Adjusted R-squared	F-statistic	Prob(F-statistic)
0.952	41.04	2.62×10^{-58}
ROI		p-value
GM Premotor cortex BA6 R		0.046
GM Superior parietal lobule 7P R		0.036
GM Primary somatosensory cortex BA1 L		0.011
GM Superior parietal lobule 5L L		0.004
FDG		
Model summary		
Adjusted R-squared	F-statistic	Prob(F-statistic)
0.963	147.3	3.40×10^{-322}
ROI		p-value
GM Inferior parietal lobule PFm R		0.044
WM Superior longitudinal fascicle L		0.044
GM Broca's area BA44 L		0.017
WM Fornix		0.015
GM Superior parietal lobule 7PC R		0.014
WM Corticospinal tract R		0.013
GM Secondary somatosensory cortex / Parietal operculum OP3 L		0.009
GM Visual cortex V5 R		0.008
WM Corticospinal tract L		0.005
GM Anterior intra-parietal sulcus hIP2 R		0.004
GM Inferior parietal lobule PGp L		0

GRAPHICAL ABSTRACT

